Regenerative Therapy 16 (2021) 53–62

Contents lists available at ScienceDirect

Regenerative Therapy

journal homepage: http://www.elsevier.com/locate/reth

Original Article

Low-temperature extrusion-based 3D printing of icariin-laden scaffolds for osteogenesis enrichment

Jian-Ting Zhang [a, *], Shan-Shan Zhang [a], Chen-Guang Liu [a], Ranjith Kumar Kankala [a, b], Ai-Zheng Chen [a, b], Shi-Bin Wang [a, b, **]

[a] Institute of Biomaterials and Tissue Engineering, Huaqiao University, Xiamen, Fujian, 361021, PR China
[b] Fujian Provincial Key Laboratory of Biochemical Technology (Huaqiao University), Xiamen, Fujian, 361021, PR China

ARTICLE INFO

Article history:
Received 24 August 2020
Received in revised form
17 December 2020
Accepted 6 January 2021

Keywords:
Extrusion-based 3D printing
Tissue regeneration
Osteogenic differentiation
Icariin
Porous scaffolds
Controlled release

ABSTRACT

Despite the accessibility to porous architectures through various biofabrication approaches for tissue engineering, incorporating various active growth regulators within their matrices that act as biochemical cues is also an essential attribute for effective tissue growth. To address these facts, icariin (ICA)-encapsulated polymeric scaffolds are fabricated using a low-temperature extrusion-based three-dimensional (3D) printing technology for efficiently promoting osteogenesis. This approach not only resulted in the generation of porous architectures but also substantially maintained the bio-efficacy of the encapsulated ICA. Moreover, these composite scaffolds based on poly(ε-caprolactone) (PCL) and tricalcium phosphate (β-TCP) encapsulated with ICA (ITP scaffolds) are systematically characterized using various techniques before and after printing. Furthermore, various investigations relevant to biodegradability, biocompatibility, ICA release, and osteogenic ability of the ITP scaffolds are explored. The intact physiochemical properties of the materials, sustained release of ICA from the scaffolds, and high biosafety at various levels ranging from cellular to animal efficiently promoted the proliferation of mouse bone marrow mesenchymal stem cells (BMSCs) and their differentiation to osteoblasts. Together, the utilization of low-temperature extrusion approach provides a convenient and eco-friendly means of fabricating highly porous 3D architectures that supply the required growth regulators in their active form for tissue regeneration.

1. Introduction

Despite the advancements in the therapeutic strategies, the repair of bone trauma and bone defects has remained as one of the most common problems in clinical medicine as the healing and repairing processes are long-term and highly complicated [1]. To this end, the field of tissue engineering holds promising potential in repairing various tissues by using the artificial biological substitutes, which restore the structure and function of the damaged tissue defects or malfunctioned organs [2–4]. Various 3D complex porous architectures as bone substitutes offer enormous advantages such as ease of tailoring size, achieve control over the microenvironment, capable of osteogenic activity by co-culturing with bone cells or its progenitor cells, and simulate the morphology and structure of bone [5–7].

Along this line, several approaches have so far been employed in the fabrication of scaffolds with porous architectures for tissue engineering applications [3]. 3D printing technology is one such promising approach resulting in geometrically distinct porous architectures in 3D orientation, which could efficiently provide control over the tissue microenvironment [8,9]. Notably, this approach also improves the physiological relevance by the printing of vital tissues and overcomes the significant limitations of conventional fabrication approaches, such as reduced reproducibility, compatibility issues relevant to porogens and organic solvents, among others [10,11]. Indeed, this technology can rapidly and accurately fabricate individualized or patient-specific tissue or organ models

* Corresponding author.
** Corresponding author. Institute of Biomaterials and Tissue Engineering, Huaqiao University, Xiamen, Fujian, 361021, PR China.
E-mail addresses: jtzhang@hqu.edu.cn (J.-T. Zhang), sbwang@hqu.edu.cn (S.-B. Wang).

Peer review under responsibility of the Japanese Society for Regenerative Medicine.

https://doi.org/10.1016/j.reth.2021.01.001

using different polymers by efficiently controlling the microstructure of materials, which can avoid the defects of immune response and allograft rejection caused by traditional organ transplantation [12–14].

Icariin (ICA), a traditional flavonoid, has recently received enormous interest from researchers for the treatment of osteoporosis [15,16]. Numerous reports demonstrated that efficient control of ICA concentration could substantially promote the differentiation of bone marrow mesenchymal stem cells (BMSCs) and the secretion of alkaline phosphatase (ALP) [17–19]. However, ICA with over high concentration could make negative effect on cell growth. In this context, Hua and colleagues fabricated polydopamine-coated scaffolds to stabilize the adsorbed ICA for bone tissue engineering [20]. The experimental results showed that scaffolds not only protected the encapsulated ICA but also facilitated the differentiation and proliferation attributes of cells. Moreover, the amount of protein secretion was significantly improved towards augmenting the osteogenic properties of the scaffolds in repairing bone tissues. Thus, preserving the highly effective amount of ICA in the scaffolds accelerates the repair of bone tissue. To this end, in the traditional, solvent-free extrusion-based printing, the printing temperature was often adjusted to a high temperature of approximately 200 °C, which might lead to the loss of bioefficacy of such sensitive growth regulators.

Inspired by these considerations, we demonstrate the fabrication of artificial substitutes with porous 3D architectures using a low-temperature extrusion-based 3D printing approach for bone tissue engineering (Fig. 1). The inks maintain fluid state at room temperature and become solid state after extruded and contacting a low-temperature (below melting point) platform, which low-temperature strategy provide the better protection of drugs or bioactive substances and is potential for further bioprinting. Herein, due to the good biocompatible and suitable mechanical properties, a combination of polymers, poly(ε-caprolactone) (PCL) and tricalcium phosphate (β-TCP) [21,22], as scaffold materials, was uniformly mixed with the growth regulator, ICA (referred as ITP scaffolds) prior to printing in anticipation of maintaining its ability of osteogenic differentiation. Further, the physicochemical, as well as mechanical properties, the release profile of ICA, biodegradability, and biocompatibility attributes of the scaffolds, were systematically investigated. Finally, the effects of ICA on the adhesion, growth, and differentiation of mouse BMSCs in the ITP scaffolds were explored by analyzing the osteogenic specific markers. This work exhibited the osteogenesis differentiation potential of ICA at an appropriate concentration. And TP scaffold was able to release drug controllably as a possible on bone regeneration material.

2. Methods

2.1. Materials

ICA was obtained from the Shenyang Long Power Technology Co., Ltd. (Shenyang, China); β-TCP powder (particle diameter of 50 μm) was purchased from the Dalian Mei Lun Biotechnology Co., Ltd. (Dalian, China). PCL polymer was purchased from the Daigang Biological Co., Ltd. (Jinan, China). Dichloromethane (DCM), 1, 4-dioxane (99.9% purity), phenol, and ethanol (99.8% purity) were purchased from the Sangon Biotech Co., Ltd. (Shanghai, China). Cell lysate, ALP assay kit, and cell counting kit (CCK)-8 were obtained from KeyGEN BioTECH. Ltd. (Nanjing, China). FITC-Phalloidin detection kit was obtained from the Beijing Solarbio Science and Technology Co., Ltd. (Beijing, China). The mouse osteocalcin (OC), Type-I collagen (Col-I), and Runt-related transcription factor 2 (Runx2) enzyme-linked immune sorbent assay (ELISA) kits were purchased from Bio-Swamp (Beijing, China). All other chemicals were of analytical purity and were used without any further purification.

2.2. Fabrication of 3D-printed scaffolds

Initially, the polymeric inks were prepared by placing 4 g of PCL and an appropriate amount of β-TCP separately in 10 mL of 1, 4-dioxane at appropriate proportions (16:1, w/w) and subsequently mixed while stirring at room temperature until resulting in a uniform dispersion. Further, the inks were deposited in the dispenser and subjected to printing using a Regenovo 3D Bio-Architect printer (Hangzhou, China) in a low-temperature mode such that the

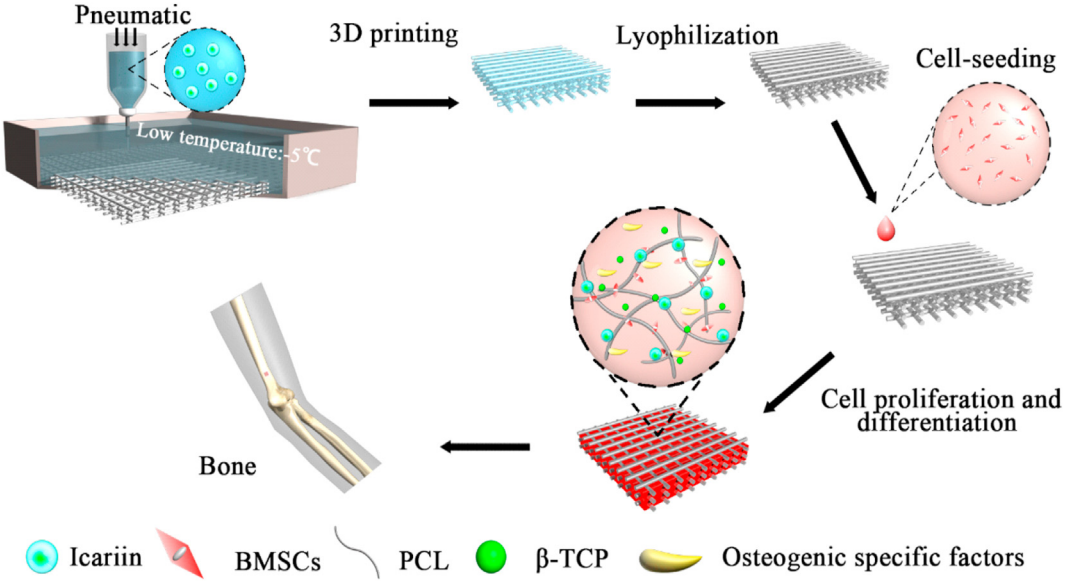

Fig. 1. Overview of the study. Schematic illustration showing the fabrication of ICA-loaded polymeric scaffolds by a low-temperature extrusion-based 3D printing approach and subsequent steps of cell adhesion, proliferation, and osteogenic properties of the composites.

scaffolds with the dimensions of 15 × 3 mm (width x height) were produced (the 3D model was built through computer-aided design (CAD)). The optimized printing conditions include the platform temperature of −5 °C, which could significantly support the formation of ink droplets after extrusion, the printing pressure of 0.1–0.15 MPa, and the printing rate of 5–8 mm/s. Finally, the 1, 4-dioxane was removed by lyophilization. These scaffolds were denoted as TP scaffolds. For fabricating ICA-loaded scaffolds, the composite inks with three gradients of ICA, 0.16, 0.32, and 0.64% of the total stent mass were prepared by dissolving an appropriate amount of ICA in the 1, 4-dioxane. These scaffolds were denoted as ITP scaffolds.

2.3. Characterization of 3D scaffolds

The surface morphology of the polymeric scaffolds was perceived by scanning electron microscope (SEM, Phenom Pro, Phenom-China, China). Fourier transform infrared spectra (FTIR, 8400S, Shimadzu, Shanghai, China), X-ray diffraction patterns (XRD, SmartLa, Rigaku Corporation, Tokyo, Japan) were recorded to explore the changes in the characteristic functional groups as well as surface crystalline transformation after 3D printing and freeze-drying, respectively. The universal material testing machine was used to explore the mechanical properties of the 3D printed scaffolds. To demonstrate the wettability attribute of the scaffolds, the contact angle was measured using the contact angle admeasuring apparatus. The instrument was equipped with a micro-syringe, for mounting an appropriate volume of 3 μL of deionized water at a rate of 0.5 μL/s every time. Further, the angle was read through a software, in which the whole process would take around 10–20 s. Further, the porosity of the fabricated scaffolds was measured by specific gravity method. The water absorption of TP stents was calculated by the weighing method.

2.4. Biodegradability

The biodegradability in vitro of the fabricated scaffolds was measured by recording the difference in their weights after exposed to phosphate-buffered saline (PBS, pH-7.4). 3D printed scaffolds (8 sets) were weighed separately and recorded the initial weight. After sterilization by UV overnight, the scaffolds were placed in 30 mL of PBS, incubated at 37 °C, and the final weights were recorded at the predetermined time intervals of 2nd, 4th, 6th, 8th, 10th, 12th, 14th, and 16th week. Furthermore, the surface morphology of these stents was observed by SEM, and the water absorption efficacy, weight loss, hydrophilicity fluctuations, and mechanical properties of the degraded scaffolds were measured. In addition, the changes in the pH value of the degradation solution were recorded at room temperature. The experiments were performed in 6 parallels in each group.

2.5. In vitro investigations

2.5.1. Cell culture

BMSCs were purchased from China Center for Type Culture Collection (CCTCC, Wuhan, China), cultured in a growth medium (DMEM supplemented with 10% FBS), and maintained in an incubator (37 °C, 5% CO_2). Fresh media were replaced every other day, and cells in the logarithmic phase were taken for subsequent experiments. The passage number of BMSCs were contained at 5–10 generation. Before cell culture, scaffolds experienced a series of sterilization process, including overnight UV exposure, anhydrous ethanol soak and air drying. Further, for better nutrient transport and cells adherent, the sterilized scaffolds were infiltrated in dioxane for 3 days.

2.5.2. Cytotoxicity of TP scaffolds during degradation

The effects of the leaching liquors of the degraded scaffolds on the growth of BMSCs were investigated. Briefly, at the fixed time points of the 2nd, 4th, 6th, 8th, 10th, 12th, 14th, and 16th week of the degradation experiment, the biodegraded scaffolds of each group were prepared at different concentrations of 10, 5, 2, and 1 mg/mL of normal cell culture medium. Further, the CCK-8 kit was used to demonstrate the toxicity of the leaching liquors to BMSCs. The proliferations of cell were calculated by relative to the negative control (e.g. cells were cultured with normal medium and tested at corresponding time points). At the corresponding time points, the expression level of ALP activity in each group was also detected by using the ALP kit. The detailed operation procedures of different scaffold extracts were performed by referring to our published reports as well as manufacturer's instructions [8,23].

2.5.3. Cytotoxicity assay of ITP scaffolds and ICA release

The ICA loading was determined by investigating the cytotoxicity and proliferation effect of ITP scaffolds with the gradient ICA concentrations on BMSCs. Initially, the leached extracts of the ITP scaffold with three different concentrations of ICA (0.64%, 0.32% and 0.16%) were prepared and fixed in a 12-well plate. BMSCs (2×10^5/well) were seeded and incubated in wells with above ITP scaffolds inside wells. Further, the CCK-8 assay was used to evaluate the cytotoxicity after incubation, at 24, 48, and 72 h. The normal TP scaffolds without ICA were employed as negative control, and ICA-saturated medium solution was used as positive control. Finally, the release behavior of ICA in ITP scaffolds was monitored by monitoring absorbance at 270 nm of supernatant for a period of 16 weeks.

2.5.4. Cell adhesion and viability assays

The adhesion, as well as proliferation rates of BMSCs on ITP scaffolds, were measured as follows. Briefly, the ITP scaffolds were sterilized and fixed in a 12-well plate for proper infiltration of cells. Further, the BMSCs with good growth state were seeded uniformly onto the scaffolds at a medium density of 2×10^5 cells. At predetermined time intervals of 1, 3, 5, 7, and 24 h after the seeding, the scaffolds were then carefully removed. Further, the cells adhered to the scaffolds were detached with 0.25% EDTA trypsin and centrifuged for 4 min at 1000 r/min. Then, the number of cells at each time point was counted with a conventional blood cell counting board, and the cell adhesion rate was subsequently calculated. Similarly, scaffolds the proliferation rates of BMSCs on scaffolds were dealt same as above. At the 1st, 3rd, 5th, 7th, and 10th day after inoculation, the cells were collected. The relative adhesion and proliferation rates were calculated by setting 6 parallels for each group (Eq. (1)).

$$\text{Cell adhesion rate } (\%) = (\text{adherent cells/seeded cells}) \times 100 \quad (1)$$

Further, BMSCs were inoculated onto ITP scaffolds in the 12-well plate at a density of 2×10^5 cells/mL. After 24 and 48 h of incubation, the scaffolds were removed, and they were then washed with PBS, fixed with 2% glutaraldehyde solution, dehydrated by alcohol gradient, and observed under SEM. In addition, the staining procedures were carried out by washing several times with PBS, fixed with 4% paraformaldehyde, stained with FITC-phalloidin for 30 min, and 4', 6-diamidino-2-phenylindole (DAPI) for 10 min in the dark, and then observed under confocal laser scanning microscope (CLSM, TCS SP5, Leica, Wetzlar, Germany).

2.6. In vivo investigations

2.6.1. Ethical considerations

All experimental procedures using animals were executed in accordance with the Experimental Animal Ethics Committee of Fujian Medical University according to the guidelines of the National Institute of Health Animal Care and the Animal Management Rules of the Ministry of Health of the People's Republic of China.

2.6.2. Hemocompatibility

Fresh anticoagulant rabbit blood was used for evaluating the hemolysis rate of leaching extracts of the printed ITP scaffolds at different concentrations (2, 5, and 10 mg/mL). The hemolysis rates of the scaffold extracts were calculated by recording the OD values of the supernatants at 545 nm using the following formula (Eq. (2)). There are 6 repetitions in each group.

$$\text{Hemolysis rate (\%)} = (\text{Sample OD at 545 nm-Negative control OD at 545 nm})/(\text{Positive control OD at 545 nm-Negative control OD at 545 nm}) \quad (2)$$

2.6.3. Acute systemic toxicity test

Male, Institute of Cancer Research (ICR) mice (20–40 g) were housed for 1 week to adapt the experimental conditions and were then randomly divided into three groups (n = 6). The experimental group of mice was intraperitoneally injected with the ITP scaffolds extracts (10 mg/mL) at a volume of 50 mL/kg (injection dose/mice weight). Further, the mice were fed for 72 h to observe the changes in diet, respiration, work as well as rest, activity, and body weight after 24, 48, and 72 h of injection. In addition, the other two groups were injected with 6.4% phenol and 0.9% saline as positive and negative controls, respectively.

Furthermore, the experimental mice were sacrificed by cervical dislocation, and then the intact livers of each group were dissected and stained with hematoxylin-eosin (HE) for histological examination. The stained tissue constructs were examined under an optical microscope to observe the pathological changes in the livers of mice.

2.7. Osteogenic differentiation in vitro

BMSCs harvested in the logarithmic phase were inoculated onto the sterilized scaffolds and were placed in the 6-well plate (5×10^4 cells/mL). Further, the filtered extracts of different scaffolds (ITP and TP scaffolds) and media contained 0.32% (w/v) ICA were collected after 7 days of culture. The calcium node formation was then observed under the optical microscope following the manufacturer's instructions. Similarly, BMSCs were inoculated and cultured, as mentioned above (refer to 2.5.1). On the 3rd, 5th, and 7th day after culture, the contents of OC, Col-I, and Runx2 were detected by using the respective ELISA kits following the manufacturer's instructions. The preparation methods of different extracts are the same as above.

2.8. Statistical analysis

All results subjected to significance tests were presented as the mean ± standard deviation (n = 3). The statistical analysis of all the experimental data was performed using GraphPad Prism (Version 7.0, GraphPad Software, San Diego, CA, USA). Analysis of variance (ANOVA) single-factor analysis was conducted at a defined level of statistical significance as $P < 0.05$, using SPSS (Version 18, IBM, Armonk, USA).

3. Results and discussions

3.1. Characterizations

In this study, the scaffolds ($15 \times 15 \times 3$ mm^3 in size) with controllable morphology and high porosity were fabricated using a low-temperature extrusion-based 3D printing approach for bone tissue engineering application (Fig. 2A-i). It was evident from the SEM observations that the fabricated 3D printed scaffolds resulted in the rough and highly porous surface, which could be highly conducive for cell adhesion and growth (Fig. 2A-ii, iii). The FTIR spectra exploring the characteristic functionalities of the polymeric materials after 3D printing and freeze-drying illustrated no signs of changes in the characteristic absorption peaks of the materials, demonstrating the compatibility of these processes with the utilized raw materials in fabricating porous architectures (Fig. 2B) [24]. Similarly, the XRD patterns also indicated that the basic reflection peaks attributed to the polymeric crystalline structures had shown no noticeable changes in their arrangement compared to that of the spectrum of the raw materials (Fig. 2C). However, the intensities of the peaks were slightly reduced, which could be due to the introduction of β-TCP, which result was similar to other composite scaffolds [25]. Together, the chemical functionalities and crystalline patterns of the resultant materials showed that the prepared TP scaffolds basically maintained the physical and chemical properties of the materials. Meanwhile, the porous structure could be highly conducive for cell growth.

Initially, the water absorption rate of TP scaffolds within 24 h was examined. As depicted in Fig. 2D, the water absorption rate of the scaffolds increased proportionally in the first 12 h of the study, and attained equilibrium state after 12 h. To further demonstrate the wettability of the TP scaffolds, the contact angle is measured, which is an important parameter that indicates the hydrophilic properties of the material. It should be noted that the smaller the value of the contact angle, the better the hydrophilicity of the scaffolds. In this case, the eventual TP scaffolds resulted in slightly less than 90° (i.e., 89.32), attributing to the hydrophilicity of the polymer (Fig. 2E). Although the fabricated TP scaffolds were mainly composed of the hydrophobic PCL material, a small amount of β-TCP evacuated well in PCL, resulting in a slight change in the polar group configuration and surface energy polarity components. These consequences would have certainly resulted in the improved overall hydrophilicity of the scaffolds. Notably, such hydrophilic surfaces could offer an excellent affinity to cells, which would make them conducive to adhesion, growth, and proliferation of cells.

Indeed, the porosity attribute of any material substantially reflects its density and mechanical properties. In this context, the mechanical properties of such material are often inversely relative to its porosity. Thus, to examine the mechanical properties of the TP scaffolds, the compressive strength of the scaffolds with the increase of the porosity and layer thickness of the 3D porous scaffold was determined (Fig. 2F). It was observed that the compressive strength of the stent amplified with the thickness, while it decreased with the increase of porosity (Fig. 2G). Based on previous preparation experience and considerations from literature, the relation between the porosity as well as the compressive strength of the scaffold could be essentially resolved in regard to the size of the scaffold under the same preparation conditions and materials [8,23,26]. Hence, based on the investigation of each parameter, the scaffolds with size of $15 \times 15 \times 3$ mm^3 were selected for the further

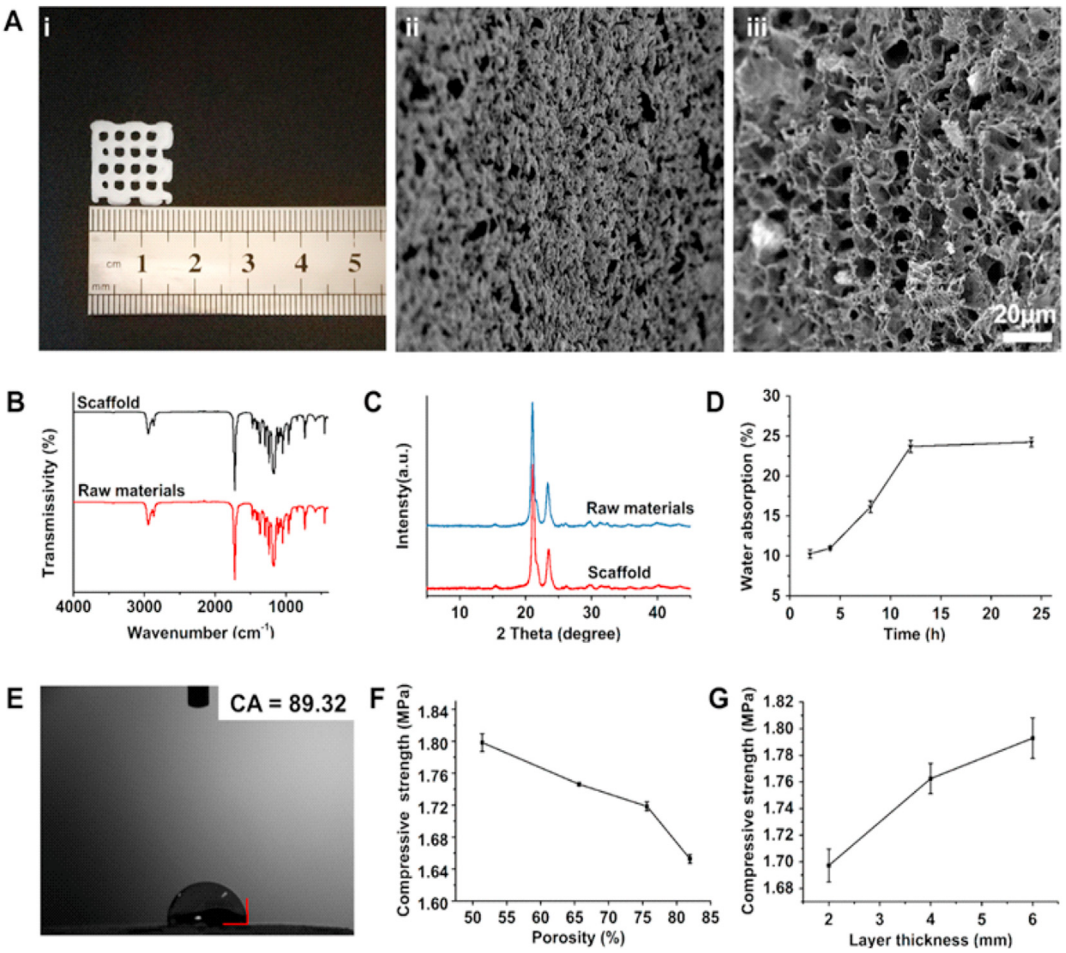

Fig. 2. Physical characterizations of 3D printed scaffolds. (A) Representative i) optical image, and SEM micrographs showing the ii) surface and iii) interior morphology of the TP scaffolds (scale bar: 20 μm). (B) FTIR spectra and (C) XRD spectra of the TP scaffolds as well as the raw materials. (D) Water absorption rate and (E) contact angle of the TP scaffolds. Effect of (F) porosity and (G) thickness on the compressive strength of TP scaffolds.

experiments, where their porosity and compressive strength were determined at 80.17 ± 4.03% and 1.78 ± 0.0153 MPa respectively.

3.2. Biodegradability of TP scaffolds

The degradation of composite scaffolds is an important attribute to be considered in bone tissue engineering as it plays a significant role throughout the process of material culture, implantation, and bone healing by affecting the transfer and metabolism of nutrients, as well as the regeneration of damaged tissues [27,28]. Therefore, it is required to study the degradation process of the composite scaffolds and whether or not the resultant degradation products would affect the normal physiological activities in the living system. As shown in Fig. 3A, the TP scaffolds were degraded in the biomimetic environment in vitro, and the pH of the solution gradually decreased from 7.4 to a weakly acidic state over time owing to the hydrolysis of ester groups of β-TCP and PCL, resulting in the acidic environment [22]. However, this attribute may have no significant influence upon implanting these substitutes as the human body is a perfect buffer system, which gradually infiltrates the acidic constituents into the surrounding tissues as well as neutralizes by acid-base balance and excretes them over time by various self-defense mechanisms [29]. Meanwhile, numerous hydrophilic groups such as carboxyl and hydroxyl groups on the main chain had significantly facilitated the water absorption performance of the degradation scaffolds (Fig. 3B). Similarly, the weight-loss rates of the stents were also constantly continued to upsurge (Fig. 3C). Moreover, as the degradation time prolonged, the mechanical properties of the degraded stents were gradually reduced (Fig. 3D). It was observed from the SEM images that the increase in the degradation time had resulted in the larger pores on the surface of the scaffolds, and even some of the structures were collapsed (Fig. 3E). Such changes might increase the contact surface between the scaffolds and the degradation fluid, which would penetrate into the scaffolds and accelerate the degradation of surrounding materials. Furthermore, the contact angle of the corresponding scaffolds with the increasing degradation time was measured. Interestingly, it was observed that the contact angle of the stent was reduced, which might be due to the enriched hydrophilic groups exposed on the main chain of the polymer, attributing to the non-uniform porous surface of the scaffolds (Fig. 3F). Collectively, these scaffolds with improved hydrophilicity and degradability attributes could efficiently promote the adhesion of cells.

3.3. Biocompatibility of 3D scaffolds

Indeed, the biocompatibility of any material generally refers to its property of exhibiting no critical responses, i.e., either toxic or immunological, when exposed to living tissues. It should be noted

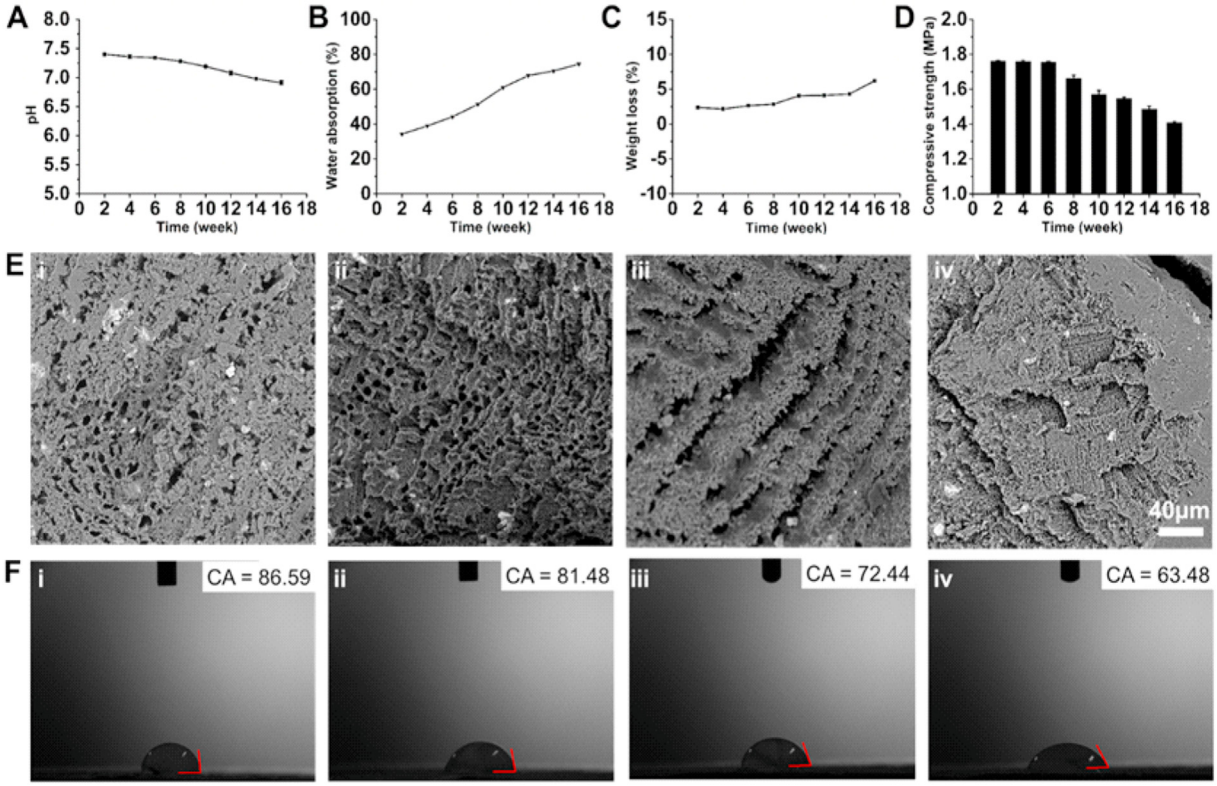

Fig. 3. Biodegradation behavior of TP scaffolds in vitro. Graphs showing the changes in (A) pH value, (B) water absorption, and (C) weight loss of the scaffolds during degradation in vitro. (D) Changes in the mechanical properties of the scaffolds during in vitro degradation (n = 3). Changes in (E) morphology and (F) contact angle of the degraded TP scaffolds in PBS solution: i) 4, ii) 8, iii) 12, and iv) 16 weeks in PBS solution. (n = 3).

that all the biomaterials used in the field of medicine should meet the guidelines of biological safety procedures related to biocompatibility. In general, the toxic effects of the fabricated scaffolds are measured by treating the cells in vitro with their leaching liquors containing the degradation products at different degradation times. To demonstrate these facts, the biocompatibility of the fabricated scaffolds was assessed by exposing them to BMSCs. As depicted in Fig. 4A, the CCK-8 assay results had shown no obvious cytotoxic effects on the cells, indicating that these stents were highly compatible and safe. Moreover, the degradation products of TP scaffolds with different degradation times also promoted the expression of ALP, indicating that the degradation products of TP scaffolds would improve the ossification of BMSCs (Fig. 4B).

Indeed, it was evident from the literature that the ICA loading played an important role in promoting or inhibiting the proliferation and differentiation of osteoblasts [18–21,26]. In view of this fact, three gradient concentrations of ICA in the scaffolds were chosen along with the normal medium as the negative control, and the medium containing 0.64% phenol as the positive control. Fig. 4C depicted that the scaffolds with different concentrations of ICA showed no significant cytotoxicity toward BMSCs. Combined with the effects of cell proliferation, the scaffolds with 0.32% content expressed the significant proliferation efficacy due to ICA was released slowly and promoted cell growth at an appropriate concentration, which was chosen as the optimal load for further experiments. Further, the ITP scaffolds have shown the sustained release of ICA without any signs of burst release, indicating that the ICA was evenly distributed throughout the 3D polymeric framework of ITP scaffolds. Moreover, the slow release could also be facilitated through gradual degradation (Fig. 4D). Notably, the uniformly dispersed ICA in the ITP scaffolds not only maintained the content of ICA exposed in the surrounding environment but also appropriately ensured the ICA persistence in its role of promoting bone formation.

Further, to evaluate the adhesion behavior of cells over ITP scaffolds, the cells were observed under the microscope, and the relative proliferation of co-loaded cells was measured. First, the cell adhesion rate of ITP scaffolds increased with time in 24 h of culture, and was indeed stable for 7 h, reaching the affinity to around 88.33%. The results could be attributed that the porous architectures generated by 3D printing technology increased the cell affinity with scaffolds by increasing the direct contact space between scaffold and cells.

Moreover, the surface and interior of the scaffolds exhibited the rough 3D surface and multi-cavity internal structure due to the volatilization of 1, 4-dioxane [30], which increased the possibility of cell attachment (Fig. 4E). Simultaneously, the cells adhered to the ITP scaffolds resulted in the augmentation of the proliferation, which could be explained by the fact that appropriate exchange of nutrients for cell growth through porous architectures [31], and the sustained release of dispersed ICA in the scaffolds (Fig. 4F). Moreover, it could be observed from the results that the cells were fully stretched and naturally grown in a fusiform or elliptical shape on the ITP scaffolds, and even the prosthetic feet were closely interdependent with the scaffolds (Fig. 5). Within 48 h of incubation, the cell number of BMSCs on ITP scaffolds was increased, indicating that the ITP scaffolds provided a conducive microenvironment for cell proliferation.

To further demonstrate the biocompatibility of ITP scaffolds, the hemolysis experiments ex vivo was performed using the fresh rabbit blood. Different concentrations of ITP scaffold extracts (2, 5, and 10 mg/mL) were separately added with fresh anticoagulant

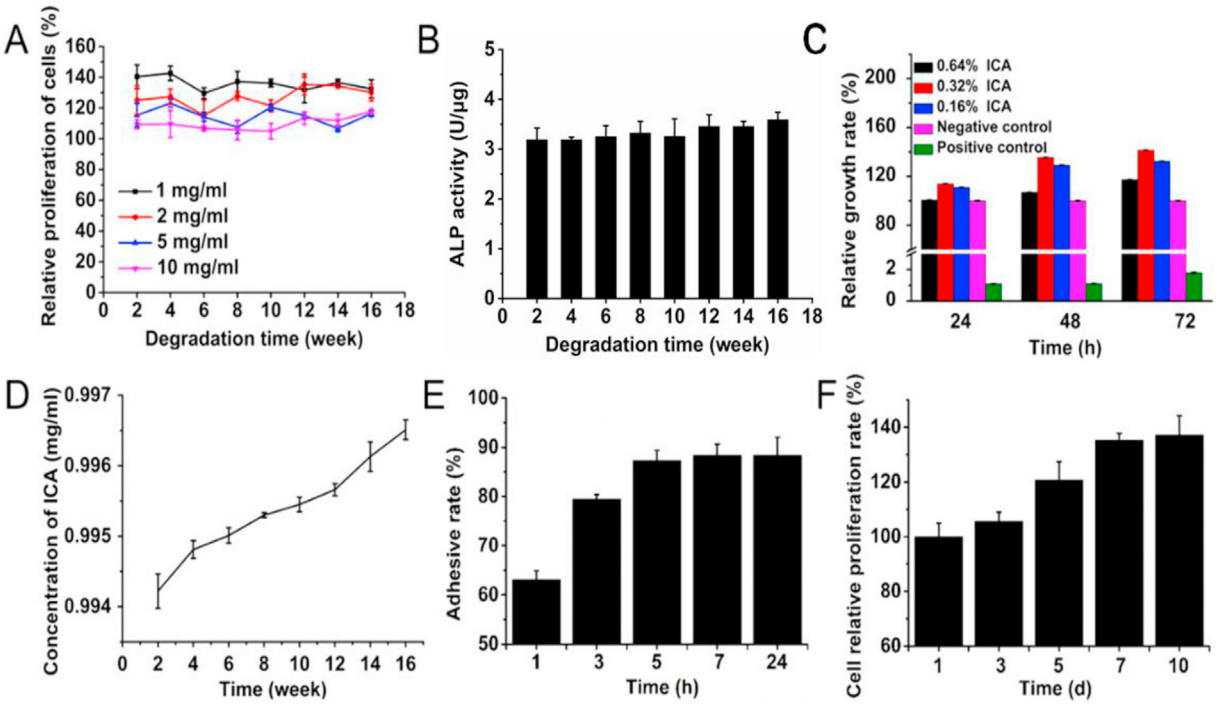

Fig. 4. Biocompatibility of scaffolds. Effects of degradation products with different degradation time on (A) cytotoxicity and (B) ALP activity (n = 6). Cell adhesion efficacy and activity of ICA/β-TCP/PCL (ITP) scaffolds. (C) The cytotoxicity of BMSCs after treatment with the extracts of scaffolds at different time intervals. (D) The accumulated release of ICA from the ITP scaffolds. Graphical representation showing the (E) adherence efficiency, and (F) relative growth rate of BMSCs on ITP scaffolds at different exposure time points (n = 6).

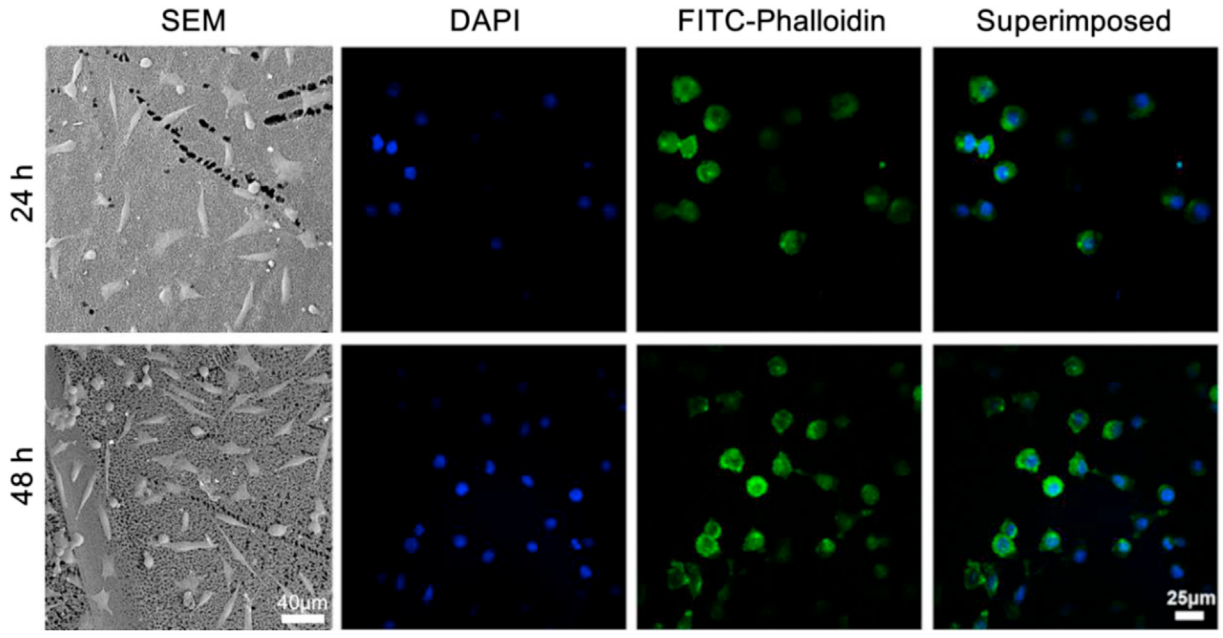

Fig. 5. Adhesion rate of cells on ITP scaffolds. BMSCs were cultured on ITP scaffolds for 2 days. The cells on the scaffolds with nuclei stained by DAPI (blue) and cytoskeleton stained by FITC-Phalloidin (green). SEM images representing the adhesion of cells onto the ITP scaffolds after incubation for 24 and 48 h. CLSM images of BMSCs cytoskeleton showing that the cells were effectively deposited on ITP exposed to various time intervals.

rabbit blood, and the absorbance values at 545 nm were then detected by an enzyme-labeled instrument (ThermoFisher Scientific, Waltham, USA). Even at the concentrations were pretty high, the hemolysis rate was far below the standards of biosafety requirements, revealing that these ITP scaffolds are highly compatible (Fig. 6A). These experimental results of high hemocompatibility of the fabricated scaffolding systems could be due to the biocompatible materials, PCL as well as β-TCP in the ITP scaffolds.

Similarly, to verify the toxicity of ITP scaffolds, acute systemic toxicity tests were performed on 18 male mice of ICR level. The common observation indices of each group of animals recorded during the experimental period were shown in Table 1. The

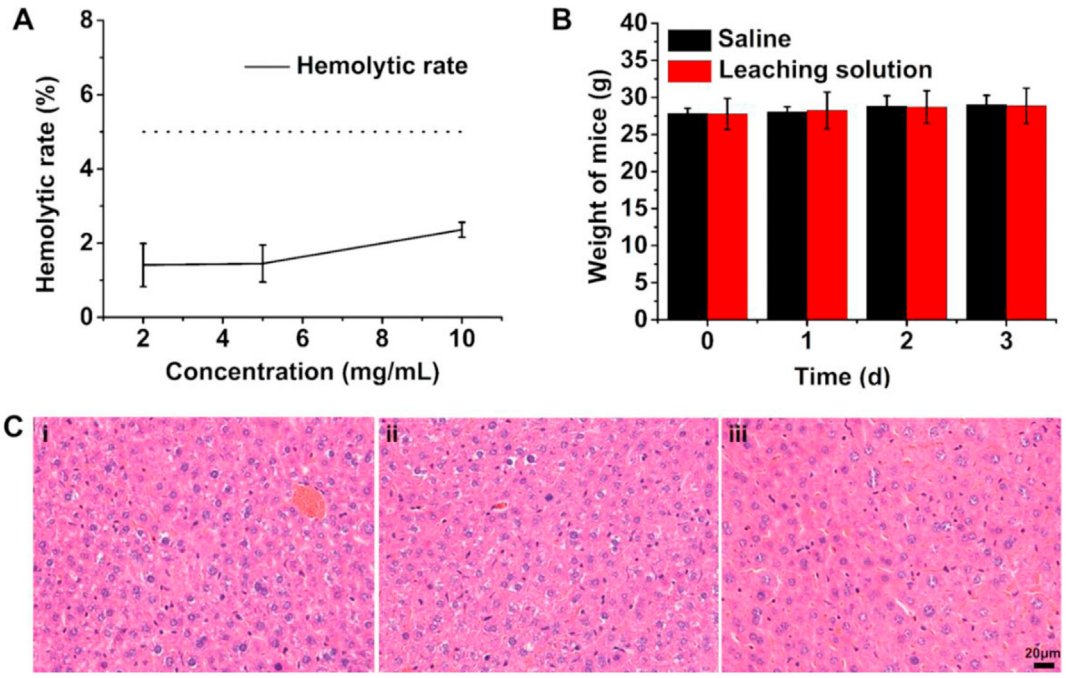

Fig. 6. Ex vivo and in vivo toxicity test results. (A) Hemolysis rate of different concentrations of ITP scaffold extracts, (B) weight changes of mice in each group during the experiment, and (C) the pathological characteristics of liver were observed after intraperitoneal injection: i) positive control, ii) negative control, and iii) experiment group. (n = 6).

experimental results were consistent in both the experimental group as well as the negative control group, indicating that the mice had no abnormal activities, and the life and rest states were good, and the body weight of the mice increased steadily during the experimental period (Fig. 6B). Contrarily, the positive control mice developed shortness of breath within 1 h of the injection and were accompanied by difficulty in breathing, convulsions, and then died. Together, it could be inferred from this experiment that ITP scaffolds have shown no significant adverse effects on the average survival of mice.

Further, after 3 days of the administration, the mice were sacrificed by cervical dislocation, and their intact liver sections were fixed with 4% paraformaldehyde solution. After hematoxylin and eosin (H&E) staining, the microscopic observations of the liver biopsies resulted that the hepatic lobules in each group were slightly hexagonal with a clear structure, and the hepatocytes were arranged radially around the central vein. In the positive control group, the central and portal veins were slightly dilated and congested. In addition, there were individual necrotic foci in the hepatic lobule, accompanied by a few fibroblast proliferations around the portal bile duct (Fig. 6C-i). Contrarily, no degeneration and necrosis of hepatocytes, no infiltration of inflammatory cells in hepatic lobules and portal ducts, and no proliferation of fibrous tissue were observed in the experimental group and the negative control group (Fig. 6C-ii, iii). It could be concluded that the materials used in the experimental group had shown no significant toxic effects on the liver.

3.4. Osteogenic differentiation in vitro

BMSCs are multifunctional stem cells in bone marrow, which can be induced to differentiate into osteoblasts by using some bioactive factors or other drugs such as dexamethasone. To evaluate the osteogenicity of ITP scaffolds, the expressions of some osteogenic specific factors were determined, which could be correlated to the process of bone formation. In the vein, calcium nodule, a diamond-like crystalline product of calcium and the predominant constituent of bone, is one of such markers that can incidentally reflect the degree of differentiation of BMSCs into osteoblasts (Fig. 7A). Different culture solutions containing 3D scaffolds showed different amounts of calcium nodules after 1-week of incubation time with BMSCs. It could be observed from Fig. 7A that enormous pink-colored diamond-like calcium nodule products were observed in the experimental group (Fig. 7A-ii, and iv) compared to the negative control group (Fig. 7A-i), Which could be attributed to the common osteogenic properties of PCL and β-TCP in the scaffold. However, a slight difference in the levels of calcium was observed in the scaffolds group due to the sustained release of ICA from the ITP scaffolds, where the concentration of ICA in medium was low and promoted differentiation of BMSCs. In comparison, ICA alone in the culture solution reduced the growth and proliferation of cells, where the over-high concentration of ICA directly contacted with BMSCs, which was consistent with the conclusions mentioned above (Fig. 7A-iii).

In addition to the overexpression of ALP, BMSCs also synthesized and secreted a large number of bone matrix substituents during

Table 1
Physiological responses of mice in each group during the experiment.

Sample	Appetite	Diarrhea	Activity	Drowsiness	Weight	Death
Positive control	–	–	Tremble and twitch	–	–	Yes
Negative control	Normal	No	Normal	No	Increase	No
10 mg/mL	Normal	No	Normal	No	Increase	No

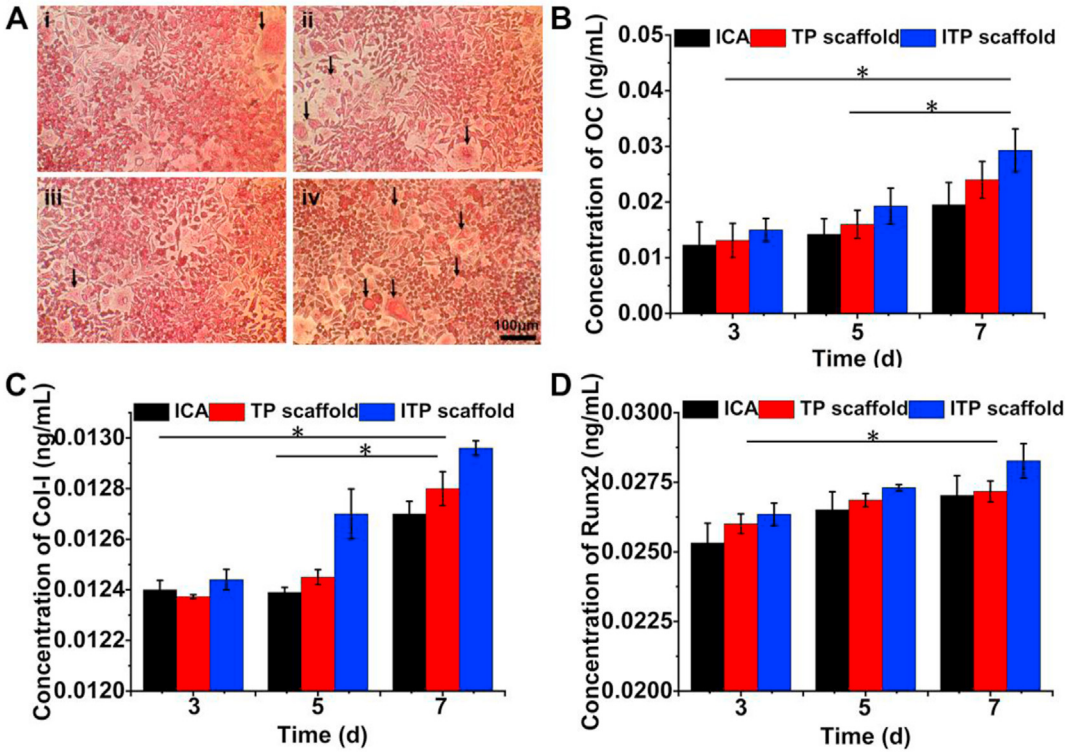

Fig. 7. Osteogenic differentiation of ITP scaffolds in vitro. BMSCs were cultured with different scaffold extracts for 7 days (n = 3). (A) Staining results of calcium nodules: i) normal control, ii) extract of TP scaffold, iii) medium containing ICA, and iv) extract of ITP scaffold, (B) OC, (C) Col-I, and (D) Runx2 in the extract of composite scaffolds solution that has been incubated with BMSCs for various time intervals.

osteoblast differentiation, such as OC, Col-I, and Runx2 [32]. The expressions of OC (Fig. 7B), Col-I (Fig. 7C), and Runx2 (Fig. 7D) in the ICA, TP scaffold and ITP scaffolds extracts group increased over time, indicating both ICA and PCL and β-TCP released from scaffold achieved osteoblast differentiation. In addition, the ITP scaffolds extracts group was higher than those in the control group as well as TP scaffolds, indicating that the ITP scaffold extract could up-regulate the expression of osteogenic differentiation-related genes in the presence of ICA. With the increase of culture time, the expressions of OC and Col-I increased slowly and exhibited significant difference compared with control group and TP scaffold group. Together, we conclude that the ICA loaded in ITP scaffolds could not only maintain the original drug activity but also slowly release ICA in response to BMSCs, thereby augmenting their rate of osteoblast differentiation.

4. Conclusions

In summary, we successfully prepared a kind of bone scaffolds based on ICA/β-TCP/PCL materials using a low-temperature extrusion-based 3D printing approach. These materials offered excellent mechanical properties as well as hydrophilicity, biocompatibility, and osteogenesis attributes. Moreover, this approach efficiently preserved the ICA in the scaffolds, and its sustained release had resulted in pronounced bioefficacy. In addition, the 3D printed scaffolds resulted in no signs of toxic substances during the degradation process, and efficiently promoted the growth and proliferation of BMSCs. Together, the ITP scaffolds significantly up-regulated the expression of osteoblast specific-genes, confirming the successful differentiation and maturation of BMSCs into bone tissues.

Author contributions

Conceptualization, J.-T. Z., S.-S. Z., C.-G. L., and S.-B. W.; Methodology, S.-S. Z. and Q.-S. W.; Review and Editing of Final Manuscript, J.-T. Z., R. K. K., A.-Z. C. and S.-B.W.; Supervision, S.-B. W.; Project Administration, A.-Z. C. and S.-B. W.; Funding Acquisition, A.-Z. C. and S.-B. W. All authors have reviewed the manuscript and approved the final version of the manuscript.

Declaration of competing interest

The authors declare that they have no known competing financial interests or personal relationships that could have appeared to influence the work reported in this paper.

Acknowledgements

This research was funded by the National Key R&D Program of China (2018YFB1105600), National Natural Science Foundation of China (NSFC, 81971734, U1605225, and 31800794), and Program for Innovative Research Team in Science and Technology in Fujian Province University.

References

[1] Naskar D, Ghosh AK, Mandal M, Das P, Nandi SK, Kundu SC. Dual growth factor loaded nonmulberry silk fibroin/carbon nanofiber composite 3D scaffolds for in vitro and in vivo bone regeneration. Biomaterials 2017;136:67–85.
[2] Kankala RK, Zhu K, Sun X-N, Liu C-G, Wang S-B, Chen A-Z. Cardiac tissue engineering on the nanoscale. ACS Biomater Sci Eng 2018;4:800–18.
[3] Kankala RK, Zhang YS, Wang S-B, Lee C-H, Chen A-Z. Supercritical fluid technology: an emphasis on drug delivery and related biomedical applications. Adv Healthc Mater 2017;6:1700433.
[4] Chen B-Q, Kankala RK, Chen A-Z, Yang D-Z, Cheng X-X, Jiang N-N, et al. Investigation of silk fibroin nanoparticle-decorated poly(l-lactic acid)

composite scaffolds for osteoblast growth and differentiation. Int J Nanomed 2017;12:1877–90.
[5] An N, Shi Y, Jiang Y, Zhao L. Organ donation in China: the major progress and the continuing problem. J Biomed Res 2016;30:81–2.
[6] Crane GM, Ishaug SL, Mikos AG. Bone tissue engineering. Nat Med 1995;1:1322–4.
[7] Bose S, Roy M, Bandyopadhyay A. Recent advances in bone tissue engineering scaffolds. Trends Biotechnol 2012;30:546–54.
[8] Liu C-G, Zeng Y-T, Kankala RK, Zhang S-S, Chen A-Z, Wang S-B. Characterization and preliminary biological evaluation of 3D-printed porous scaffolds for engineering bone tissues. Materials 2018;11:1832 (Basel, Switzerland).
[9] Kankala RK, Zhu K, Li J, Wang C-S, Wang S-B, Chen A-Z. Fabrication of arbitrary 3D components in cardiac surgery: from macro-, micro- to nanoscale. Biofabrication 2017;9. 032002.
[10] Melchels FPW, Domingos MAN, Klein TJ, Malda J, Bartolo PJ, Hutmacher DW. Additive manufacturing of tissues and organs. Prog Polym Sci 2012;37:1079–104.
[11] Powers MK, Lee BR, Silberstein J. Three-dimensional printing of surgical anatomy. Curr Opin Urol 2016;26:283–8.
[12] Cui X, Boland T, D'Lima DD, Lotz MK. Thermal inkjet printing in tissue engineering and regenerative medicine. Recent Pat Drug Deliv Formulation 2012;6:149–55.
[13] Ozbolat IT, Yu Y. Bioprinting toward organ fabrication: challenges and future trends. IEEE Trans Biomed Eng 2013;60:691–9.
[14] Bertassoni LE, Cardoso JC, Manoharan V, Cristino AL, Bhise NS, Araujo WA, et al. Direct-write bioprinting of cell-laden methacrylated gelatin hydrogels. Biofabrication 2014;6. 024105-24105.
[15] Ma H-P, Ming L-G, Ge B-F, Zhai Y-K, Song P, Xian CJ, et al. Icariin is more potent than genistein in promoting osteoblast differentiation and mineralization in vitro. J Cell Biochem 2011;112:916–23.
[16] Xie X, Pei F, Wang H, Tan Z, Yang Z, Kang P, et al. A promising osteoinductive compound for repairing bone defect and osteonecrosis. J Biomater Appl 2015;30:290–9.
[17] Song L, Zhao J, Zhang X, Li H, Zhou Y. Icariin induces osteoblast proliferation, differentiation and mineralization through estrogen receptor-mediated ERK and JNK signal activation. Eur J Pharmacol 2013;714:15–22.
[18] He L, Yang J, Lu J, Xiao Y, Fan Y, Zhang X. Preparation and characterization of a novel hyaluronic acid–icariin conjugate hydrogel. Mater Lett 2014;136:41–4.
[19] Wu Y, Xia L, Zhou Y, Xu Y, Jiang X. Icariin induces osteogenic differentiation of bone mesenchymal stem cells in a MAPK-dependent manner. Cell Prolif 2015;48:375–84.
[20] Liu H, Li W, Luo B, Chen X, Wen W, Zhou C. Icariin immobilized electrospinning poly(l-lactide) fibrous membranes via polydopamine adhesive coating with enhanced cytocompatibility and osteogenic activity. Mater Sci Eng C 2017;79:399–409.
[21] Lobo SE, Arinzeh TL. Biphasic calcium phosphate ceramics for bone regeneration and tissue engineering applications. Materials 2010;3:815–26.
[22] Dorati R, Pisani S, Maffeis G, Conti B, Modena T, Chiesa E, et al. Study on hydrophilicity and degradability of chitosan/polylactide-co-polycaprolactone nanofibre blend electrospun membrane. Carbohydr Polym 2018;199:150–60.
[23] Kankala RK, Xu X-M, Liu C-G, Chen A-Z, Wang S-B. 3D-Printing of microfibrous porous scaffolds based on hybrid approaches for bone tissue engineering. Polymers 2018;10:807.
[24] Sharifi F, Atyabi SM, Norouzian D, Zandi M, Irani S, Bakhshi H. Polycaprolactone/carboxymethyl chitosan nanofibrous scaffolds for bone tissue engineering application. Int J Biol Macromol 2018;115:243–8.
[25] Mkhabela V, Ray SS. Biodegradation and bioresorption of poly(ϵ-caprolactone) nanocomposite scaffolds. Int J Biol Macromol 2015;79:186–92.
[26] Kankala KR, Lu F-J, Liu C-G, Zhang S-S, Chen A-Z, Wang S-B. Effect of icariin on engineered 3D-printed porous scaffolds for cartilage repair. Materials 2018;11.
[27] Lu L, Zhu X, Valenzuela RG, Currier BL, Yaszemski MJ. Biodegradable polymer scaffolds for cartilage tissue engineering. Clin Orthop Relat Res 2001;391.
[28] Manavitehrani I, Fathi A, Badr H, Daly S, Negahi Shirazi A, Dehghani F. Biomedical applications of biodegradable polyesters. Polymers 2016;8.
[29] Ara M, Watanabe M, Imai Y. Effect of blending calcium compounds on hydrolytic degradation of poly(dl-lactic acid-co-glycolic acid). Biomaterials 2002;23:2479–83.
[30] Mok S-W, Nizak R, Fu S-C, Ho K-WK, Qin L, Saris DBF, et al. From the printer: potential of three-dimensional printing for orthopaedic applications. J Orthop Translat 2016;6:42–9.
[31] Tang Y, Jacobi A, Vater C, Zou L, Zou X, Stiehler M. Icariin promotes angiogenic differentiation and prevents oxidative stress-induced autophagy in endothelial progenitor cells. Stem Cell 2015;33:1863–77.
[32] Cheng SL, Yang JW, Rifas L, Zhang SF, Avioli LV. Differentiation of human bone marrow osteogenic stromal cells in vitro: induction of the osteoblast phenotype by dexamethasone. Endocrinology 1994;134:277–86.